SAND2015-4239C

Macroscopic and microscopic lithologic controls on the mechanical properties of mudstones

Grigg[1], J., Dewers[2], T., Yoon[2], H., Mozley[1], P., Rinehart[3], A., Heath[2], J.

[1]Department of Earth and Environmental Sciences, New Mexico Tech, Socorro, NM 87801
[2]Geomechanics Department, Sandia National Laboratories, Albuquerque, NM 87185
[3] New Mexico Bureau of Geology & Mineral Resources, New Mexico Tech, Socorro, NM 87801

Acknowledgment

This work was funded by the U.S. Department of Energy, Office of Science, Office of Basic Energy Sciences under Award Number DE-SC0006883. Sandia National Laboratories is a multi-program laboratory managed and operated by Sandia Corporation, a wholly owned subsidiary of Lockheed Martin Corporation, for the U.S. Department of Energy's National Nuclear Security Administration under contract DE-AC04-94AL85000.

Macroscopic Lithofacies Interpretation: Field Methods

Abstract The performance of unconventional mudstone reservoirs is in large part a function of the mechanical properties of the mudstone. Mudstone mechanical properties are controlled by a variety of geologic variables, including detrital and authigenic mineralogy, organic content, and the spatial distribution of these characteristics (i.e., heterogeneity). We are investigating the impact of these lithologic controls across a wide range of scales for samples of the Mancos Shale obtained from a TeraTek quarry in Wyoming. We described the lithologic characteristics of the mudstone using a variety of techniques. The samples were first subdivided into principal macroscopic lithofacies. Samples of the macroscopic lithofacies were further characterized petrographically and microscopic facies were identified. Microlithofacies were further analysed using an electron microprobe (BSE, element mapping, and quantitative point analysis) to identify fine grained texture and composition, laser confocal microscopy to map the abundance, size, and spatial distribution of porosity, and microCT scanning. Mudstone mechanical properties will then be measured at a range of scales, including seismic wave velocity (Vp, Vs) and nanoindentation measurements of focused ion-beam milled pillars. Our goal is to allow more accurate prediction of reservoir performance by developing a multi-scale understanding of mudstone response to reservoir stimulation efforts.

Figure 1. The photo to the left is of the quaried Mancos Shale block refered to as the "Cheese Wheel" used in all analysis withing this project.

Figure 2. The photo to the right is of a block cut from the "cheese wheel." All analysis are from this block. All thin section are made from Slice 1. Slice 2 will be used in ion beam milling tests.

Figure 3. Above. Scan fold out of the center block of the "cheese wheel". Scans include; top-front face of slice 2, left-left sife of center block, middle-front face of slice 1, and right-right side of center block of "cheese wheel".

Figure 4. Left and below. Macroscopic lithofacies interpretation of figure 3 fold out. Legend for interpretation is to the left. Observations were made with hand lense and spray bottle.

Legend. Each color corresponds to a macroscopic lithofacies of the center block of the "Cheese Wheel".

- Interlaminated clay and silt mudstone
- Disrupted very fine sand, silt, and clay mudstone
- Parallel and ripple laminated very fine sand and silt, and clay mudstone
- Lenticular very fine sand and silt sandstone
- Parallel and ripple laminated very fine sand and silt sandstone

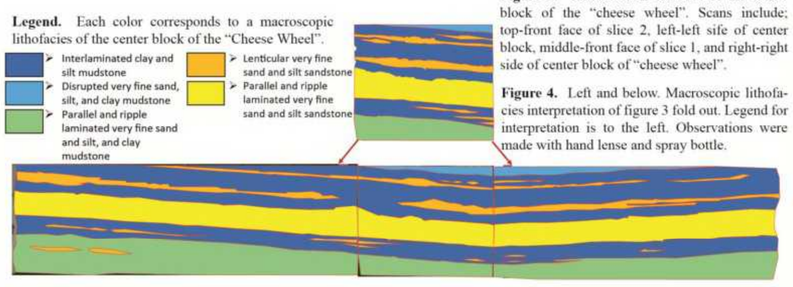

Microscopic Lithofacies Interpretation: Optical Petrography

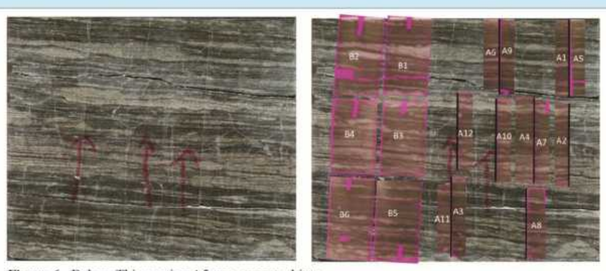

Figure 5. Left. Left scan is of front face of slice 2. Right scan is the same and includes location of thin section cut from slice 1 compared to slice 2. Thin section A1-A12 were cut perpendicular to slice 1 and 2. The position of these perpendicularly cut thin sections are represented with a scan of the right or left side of the thin section according to the side of the thin section that was originally closer to slice 2. This side is marked with a black line. Thin sections B1-B6 were cut parallel to slice 2.

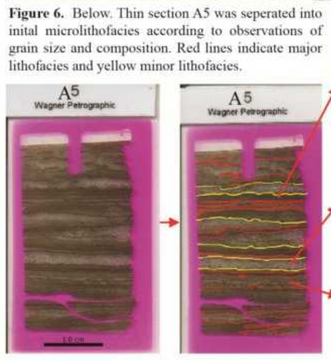

Figure 6. Below. Thin section A5 was seperated into inital microlithofacies according to observations of grain size and composition. Red lines indicate major lithofacies and yellow minor lithofacies.

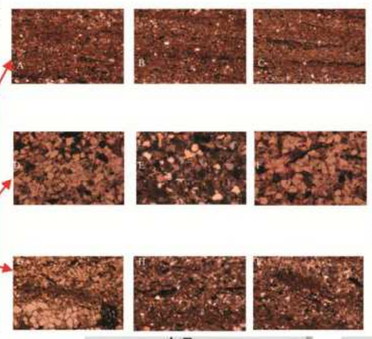

Figure 7. Left. After initial lithofacies bounderies were assigned three representative photos were taken of easy lithofacies. each photo was uploaded into JMicroVision. In JMicrovision each photo was spatialy calabrated then pointcounted for both grain size and composition. Photos A-C ore of a silt bearing, clay rich mudstone. Photos D-F are of a muddy sandstone. Photos G-I are of a Silt and clay bearing mudstone. See figure 8 for full microlithofacies interpretation of thin section A5 and see figures 9-11 for lithofacies classifications.

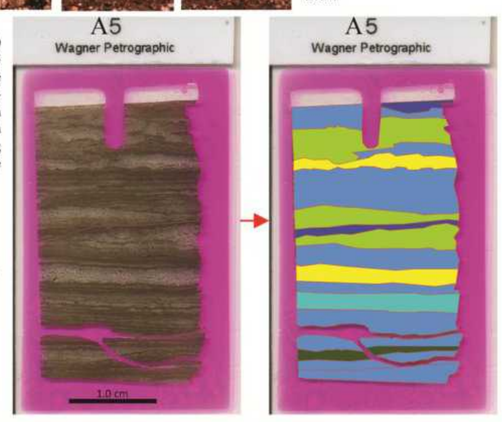

Figure 8. Right. After the seperate microlithofacies (laminations) were photographed and analized in JMIcroVision thin section A5 was reassigned lithofacies boundaries according to the results of the grain size and compositional optical analysis. Microlithofacies interprationals were then classified according to ternary diagram in figure 9. Classification skeme taken from Macquaker 2007. Each color represents a different microlithofacies classification according to grain size . For legend for the microlithofacies classification see below.

Legend. Each color corresponds to a macroscopic lithofacies of the center block of the "Cheese Wheel".

- Clay-rich mudstones
- Silt-bearing, clay rich mudstone
- Silt and clay-bearing mudstone
- Clay-bearing, silt rich mudstone
- Sand and silt-baring, clay-rich mudstone
- Sand, silt, and clay baring mudstone
- Muddy, very fine sandstones

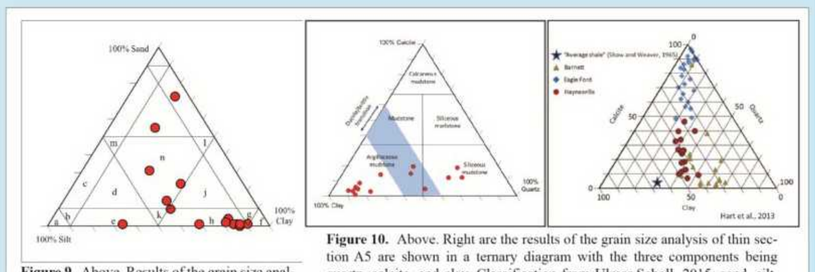

Figure 9. Above. Results of the grain size analysis of thin section A5 are shown in a ternary diagram with the three components being sand, silt, and clay. Legend for the classification shown to the right. Classification from Macquaker 2007.

Figure 10. Above. Right are the results of the grain size analysis of thin section A5 are shown in a ternary diagram with the three components being quartz, calcite, and clay. Classification from Ulmer-Scholl, 2015. sand, silt, and clay. Left compare the results of thin section A5 to industry standards.

Legend for figure 9. a)silt-dominated mudstone b)silt-rich mudstone c)sand-bearing, silt-rich mudstone d)sand and clay-bearing, silt rich mudstone e)clay-bearing, silt-rich mudstone f)clay dominated mudstone g)clay-rich mudstone h)silt-bearing, clay-rich mudstone i)sand-bearing, clay-rich mudstone j)sand and silt-bearing clay rich mudstone k)silt and clay-bearing mudstone l)sand and clay-bearing mudstone m)sand and silt-bearing mudstone n)sand, silt and clay-bearing mudstone

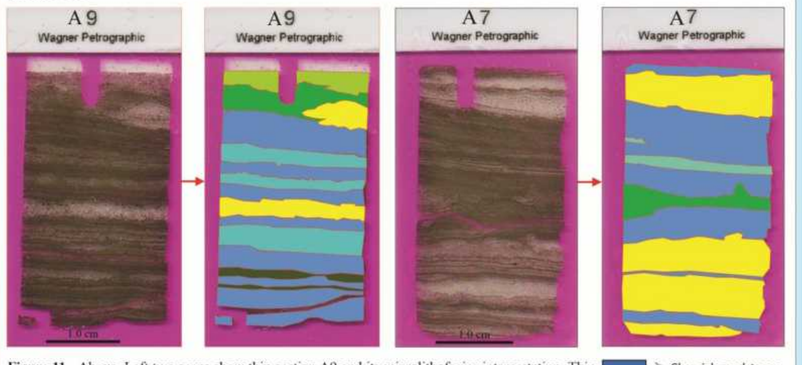

Figure 11. Above. Left two scans show thin section A9 and its microlithofacies interpretation. Thin section is from same depositional intervals as thin section A5. this shows the horizontal heterogeneity in slice 1 Compare A9 to thin section A5. Right two scans show thin section A7 and its microlithofacies interpretation. Thin section is from lower depositional intervals than thin section A5. See figure 5 for possition of thin section relative to slice 2. Legend of microlithofacies icolor map is to the right.

- Clay-rich mudstones
- Silt-bearing, clay rich mudstone
- Silt and clay-bearing mudstone
- Clay-bearing, silt rich mudstone
- Sand and silt-baring, clay-rich mudstone
- Sand, silt, and clay baring mudstone
- Muddy, very fine sandstones

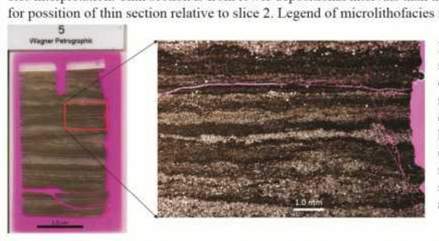

Figure 12. Right. Thin section A5 with a blowup of silt-bearing, clay rich mudstone. This lithofacies shows high internal heterogeneity which is expressed by sub millimeter inter interlaminated silt, clay, and mixed silt and clay.

Microscopic Lithofacies: MicroCT and Confocal Laser Scanning Microscopy

Figure 13. Above. A one-inch diameter core sample (left) and cross sectional micro-CT image (right).

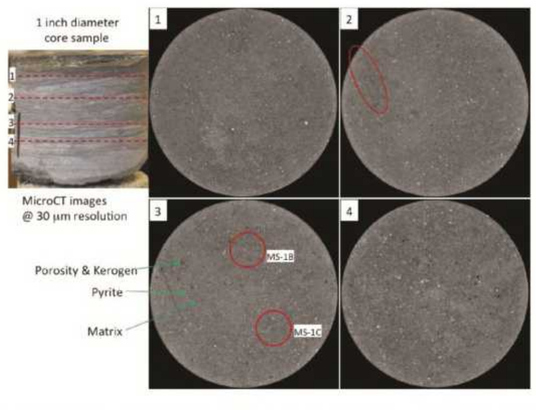

Figure 14. Four cross-sectional micro-CT images (30 micron resolution). Porosity and kerogen (black), pyrite (white grains). Fractures are evident in image 2 (circled). Circles in image 3 show two subsampled regions shown in Figures 15 and 16.

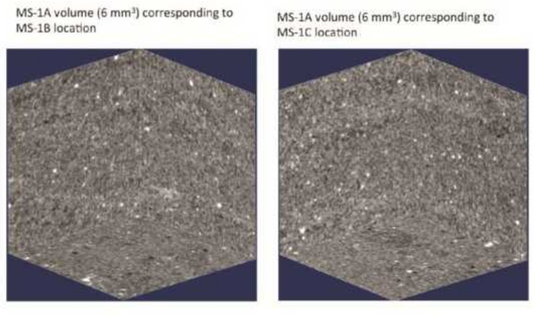

Figure 15. Above. 3D views of CT images at 30 micron resolution in regions shown in Figure 14(3).

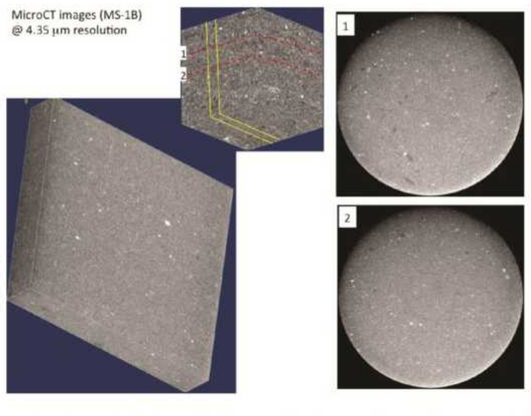

Figure 16. Above left. 3D views of CT images in MS-1B region (Figure 13(3)). Above right. Two cross sectional images with porosity and kerogen (black) and pyrite (white) grains evident. 4.35 micron resolution.

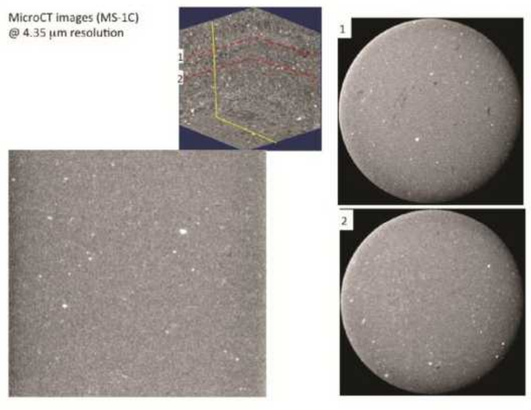

Figure 17. Above left. 3D views of CT images in MS-1C region (Figure 13(3)). Above right. Two cross sectional images with porosity and kerogen (black) and pyrite (white) grains evident. 4.35 micron resolution.

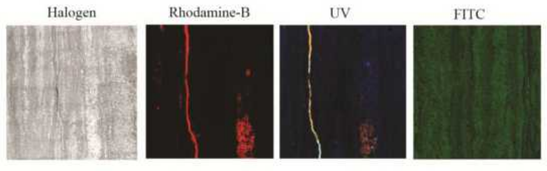

Figure 18. Laser confocal images of a thin section impregnated with rhodamine-B dyed epoxy. Images obtained using four different filter sets are shown. Fine-resolution (0.25 - 2 micron) confocal images are combined with multiscale microCT images to characterize the microlithofacies and pore networks. Feature identification techniques (e.g., multiscale texture segmentation, support vector machine) are used to identify key features of microlithofacies combined with petrographic analysis.

Conclusions and Future Work

Conclusions

The Mancos Shale samples from the "Cheese Wheel" show considerable heterogeneity both at the macroscopic and microscopic scale. Heterogeneity in the vertical direction is observed down to the sub millimeter scale and is composed of interlaminated very fine sand, silt, and clay particles. Heterogeneity in the horizontal direction is present at the cm to 10s cm scale with laminations that pinch out or transition gradually. Compositional end members quartz, calcite and clay also very considerably between lithofacies. Further investigation is necessary to understand the relationship between gemechanical behavior and lithology at the macro and micro scale.

Future Work

The work presented above will continue with lithologic description of the microlithofacies o the Mancos Shale samples from the "Cheese Wheel." Descriptive work with continue with laser confocal microscopy to map the abundance, size, and spatial distribution of porosity, and microCT scanning to characterize samples for quasi static compressive tests (before and after compression). Descriptive work will also include electron microprobe analyses (BSE, element mapping, and quantitative point analysis) to identify fine grained texture and composition. Mudstone mechanical properties will then be measured at a range of scales, including seismic wave velocity (Vp, Vs), nanoindentation measurements of focused ion-beam milled pillars, and quasi static compressive tests. Our goal is to allow more accurate prediction of reservoir performance by developing a multi-scale understanding of mudstone response to reservoir stimulation efforts.

References

MACQUAKER, J.H.S., AND ADAMS, A.E., 2003, Maximizing information from fine grained sediments: an inclusive nomenclature for mudstones: Journal of Sedimentary Research, v. 73, p. 735–744.

ULMER-SCHOLLE, D. A., SCHOLLE, P. A., SCHIEBER, J., AND RAINE, R. J., 2014, A color guide to the petrography of sandstone, siltstone, shales and associated rocks, American Association of Petroleum